Supplementary Information

Surface Grafted Polysarcosine as a Peptoid Antifouling Polymer Brush

King Hang Aaron Lau,[a,b] *Chunlai Ren,*[c] *Tadas S. Sileika,*[a,b] *Sung Hyun Park,*[a,b] *Igal Szleifer*[a,b,d-f]*, *Phillip B. Messersmith*[a,b,e-h]*

[a]Department of Biomedical Engineering, [b]Chemistry of Life Processes Institute, Northwestern University, Evanston, Illinois 60208, USA

[c]National Laboratory of Solid State Microstructures, Nanjing University, Nanjing 210093, China

[d]Department of Chemistry, [e]Department of Chemical and Biological Engineering, [f]Robert H. Lurie Comprehensive Cancer Center, [g]Institute for Bionanotechnology in Medicine, [h]Department of Materials Science and Engineering, Northwestern University, Evanston, Illinois 60208, USA

AUTHOR EMAIL ADDRESSES: aaronlau@northwestern.edu, chunlair@nju.edu.cn, tadassileika2009@u.northwestern.edu, parksh@northwestern.edu, igalsz@northwestern.edu, philm@northwestern.edu

*Corresponding authors: igalsz@northwestern.edu, philm@northwestern.edu

Contents:

1. Molecular volumes of sarcosine polymers 3
2. Water Contact Angles of PSAR-10 Brush Surface over a Range of Chain Densities 4
3. Comparison of fibrinogen (Fg) adsorption on PSAR-20 and on other surface grafted polymer brushes 5
4. Comparison of fibroblast mammalian cell attachment adsorption on PSAR-20 and on POEGMA surface grafted polymer brushes 7
5. AFM measurements on TiO_2 (in air) and on PSAR-20 brush (in aqueous solution) 9
6. Adsorption measurements on PSAR-20 samples immersed in 10% bovine serum 12

References 13

1. Molecular volumes of sarcosine polymers

To calculate the volumes of the sarcosine, DOPA, and lysine monomer units in the PSAR chains, a molecular dynamics (MD) simulation was carried out for PSAR-20 chains grafted on TiO_2 surface, and the final chain configurations were taken to calculate the monomer volumes using the VOIDOO software package.[*] Briefly, 29 PSAR-20 chains were generated and grafted to a non-hydroxylated rutile (110) TiO_2 crystal surface via a hydrogen atom of the terminal DOPA residue in random distribution at surface chain density of 0.72 nm^{-2}. The simulation box was then filled with explicit TIP4P water molecules and Cl^- counter ions, and the system was first energetically stabilized by the steepest descent algorithm, followed by a production run for a 100-ns MD simulation at temperature 300K with constant volume. The MD simulation was run using the GROMACS simulation package, version 4.5.4.[†] All atoms in the TiO2 surface were kept static during the simulation for computational efficiency. The OPLS force field was used to model the PSAR-20 chains,[‡] and the atomic formal charges and the Lennard-Jones parameters of Ti and O atoms were taken from Kang et al.[§] The final PSAR-20 chain configurations from the MD simulation were then used as an input of the VOIDOO software package to calculate the average volumes of the sarcosine, DOPA, and lysine monomer units. The VOIDOO software package generates a 3D cubic grid of points in space and uses the van der Waals radii of atoms to identify the points enclosed by the molecules. The program runs a loop in which the spacing between grid points decreases in each successive cycle, and the final volume is determined when the volumes from two consecutive loops converge within a given threshold of 0.1%. The calculated volumes are:

DOPA: 0.1947 nm^3

Lysine: 0.1608 nm^3

Sar: 0.0876 nm^3

PSAR-10: 1.76 nm^3

PSAR-20: 2.64 nm^3

[*] G.J. Kleywegt and T.A. Jones, Acta Cryst., D50, 178-185 (1994)

[†] B. Hess, C. Kutzner, D. van der Spoel, and E. Lindahl, J. Chem. Theory Comput., 4, 435-447 (2008)

[‡] S.H. Park and I. Szleifer, J. Phys. Chem. B, 115, 10967-10975 (2011)

[§] Kang, X. Li, Y. Tu, Q. Wang, and H. Agren, J. Phys. Chem. C, 114, 14496-14502 (2010)

2. Water Contact Angles of PSAR-10 Brush Surface over a Range of Chain Densities

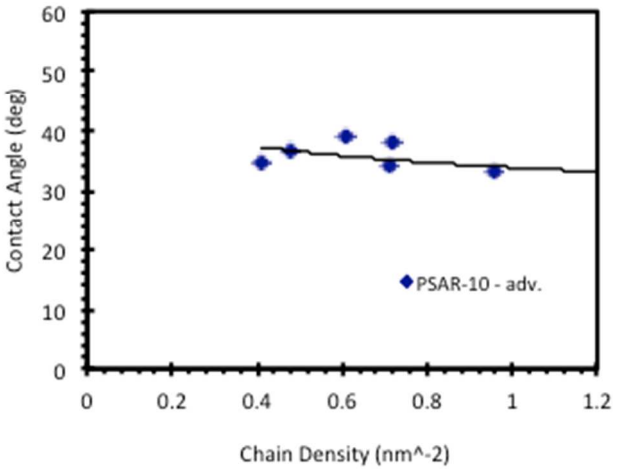

Figure S1. Advancing water contact angle measured on PSAR-10. The receding angles over the entire experimental range of chain densities were at or below 5°.

3. Comparison of fibrinogen (Fg) adsorption on PSAR-20 and on other surface grafted polymer brushes

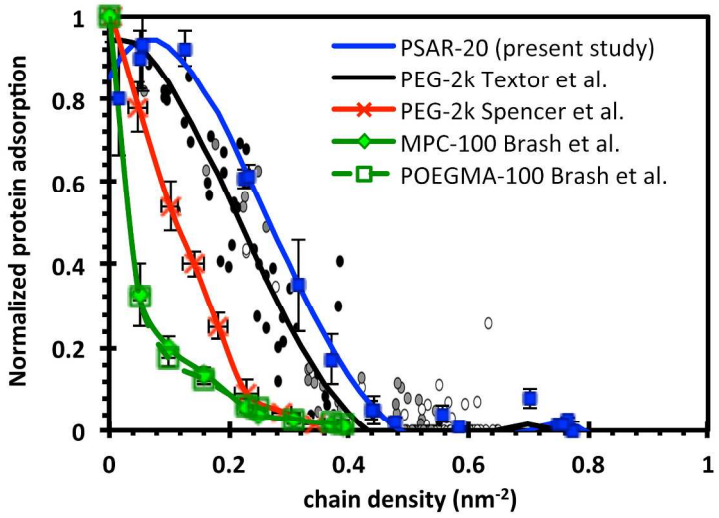

Figure S2. (A) Fibrinogen (Fg) adsorption as a function of grafted chain density, on PSAR-20, methoxy-terminated PEG-2k grafted via two methods, and on acrylate graft polymers with phosphorylcholine (MPC-100) and oligo(ethylene glycol) sidechains (POEGMA-100). The polymer brush systems, and the molecular weights of their respective brush sections, are (identified by the color of the plotted series): Blue - PSAR-20 present study (M_w = 1.46 kDa; degree of polymerization (d.p.) = 20); Black/gray - PEG-2k Textor et al.[1] (M_w ~ 2 kDa, d.p. ~ 45, poly(ethylene glycol) grafted with catechol functionalized polylysine anchor design); Red – PEG-2k Spencer et al.[2] (M_w ~ 2 kDa, d.p. ~ 45, poly(ethylene glycol) grafted with polylysine anchor design); Green diamonds – MPC-100 Brash et al.[3] (M_w ~ 28 kDa, d.p. ~ 100, surface initiated graft polymers of 2-methacryloxyethyl phosphorylcholine); Green open squares – OEGMA-100 Brash et al.[3] (M_w ~ 30 kDa, d.p. ~ 100, surface initiated graft polymers of oligo(ethylene glyocol) methyl ether methacrylate). (B) For PEG-2k Textor et al. the data points in various shades of gray represent PEG grafting under different conditions; the black curve is a spline fit to guide the eye only. For the purpose of comparison, the data obtained by the different research groups are normalized to the adsorbed Fg mass densities measured on the respective unfunctionalized control substrates. In the present study, this was 521 ng/cm^2 on TiO_2; for the work of Textor et al., this was 540 ng/cm^2 on TiO_2; for the work of Spencer et al, this was 320 ng/cm^2 on TiO_2; for the work of Brash et al., this was 570 ng/cm^2 on polymerization initiator coated silicon wafer. The error bars indicate ±1 SD.

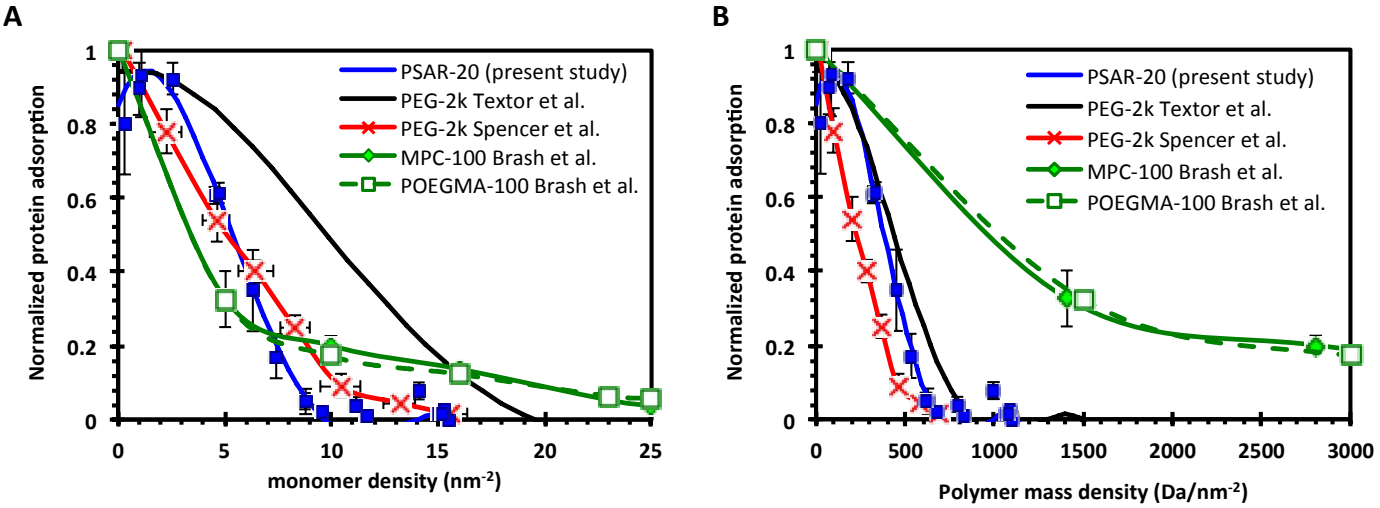

Figure S3. Comparison of fibrinogen (Fg) adsorption on PSAR-20 with that on PEG-2k, and on acrylate graft polymers with phosphorylcholine (MPC-100) and oligo(ethylene glycol) sidechains (POEGMA-100). Details of the polymer systems are described in the caption of Figure S3. (A) The data is plotted as a function of the monomer density, obtained by multiplying the grafted chain density with the degree of polymerization. (B) The data is plotted as a function of the polymer mass density, obtained by multiplying the grafted chain density with the polymer molecular weight. The error bars indicate ±1 SD.

The amount of fibrinogen adsorbed on the PSAR-20 grafted polymer brush is compared in Figures S2 and S3 with the adsorption on a number of frequently studied grafted polymer brushes for which adsorption data as a function of grafted chain density is available. The comparison is made with poly(ethylene glycol) (PEG), and with the acrylate graft polymers with oligo(ethylene glycol) (POEGMA-100) and zwitterionic phosphorylcholine (MPC-100) sidechains. Details of the polymer systems and references to the different studies are listed in the caption of Figure S2.

The molecular weight of the 20-mer PSAR-20 chain is 1.4 kDa, which is 30% lower than the 45-mer 2 kDa PEG, and 95% lower than the 100-mer MPC-100 and POEGMA-100. Higher grafted surface chain densities and longer polymer chain lengths, both of which contribute to a higher surface density of grafted polymer material, are recognized to be the main determinants in enhancing the performance of polymer brushes in resisting protein adsorption.[4-6] Therefore it is expected that the lower molecular weight and shorter PSAR-20 would resist fibrinogen adsorption less than the particular PEG, MPC and OEGMA brushes shown in Figure S2 (the curve for PSAR-20 lies to the right of the other polymer series). For a fairer comparison, the polymer chain length is controlled for by plotting the adsorption data as a function of the monomer density instead (Figure S3A, obtained by multiplying the chain density with the degree of polymerization). Further, differences in the monomer molecular weight may be controlled for by plotting the adsorption data as a function of grafted polymer mass density (Figure S3B, obtained by multiplying the chain density with the polymer molecular weight). However, the latter normalization implies that the steric bulk of the polymer has a primary effect on the antifouling performance.

As shown in Figure S3, PSAR-20 compares favorably with PEG, MPC and POEGMA in its resistance against fibrinogen adsorption. The critical monomer density for essentially completely inhibiting fibrinogen adsorption is actually the lowest for PSAR-20 (~10 nm^{-2}; Figure S3A). The data for PSAR-10 overlaps with the PSAR-20 series (not shown). In comparison, the critical density is in the range of 12 to 19 nm^{-2} for PEG. For MPC and POEGMA, although the initial drop in fibrinogen adsorption with a small density of chains grafted is the sharpest among the polymers considered here, the inhibition in protein adsorption at intermediate grafting densities is relatively ineffective, and the critical inhibitory monomer density is > 25 nm^{-2}. If the resistance against fibrinogen adsorption is compared as a function of grafted polymer mass density (Figure S3B), the trend for PSAR-20 lies in between the two data sets obtained for PEG, and both the PSAR and PEG apparently resist fibrinogen adsorption at significantly lower mass densities than MPC and POEGMA. This latter observation may simply reflect the fact that the MPC and OEGMA monomer units have a much higher mass than those of PSAR and PEG (SAR monomer = 71 Da; EG monomer = 44 Da; MPC monomer = 281 Da; OEGMA monomer ~300 Da).

However, the above comparison must be treated with caution, as it also reflects performance differences resulting from differences in the polymer grafting methodology, and differences in the experimental conditions. As illustrated by the two data series for PEG ("PEG-2k Spencer et al." and "PEG-2k Textor et al.), a large discrepancy may exist between two sets of experiments employing the same polymer but using different grafting strategies—although both experiments used TiO_2 substrates, "PEG-2k Spencer et al." utilized a polylysine grafting segment while "PEG-2k Textor et al." used a polylysine segment that is further functionalized with adhesive catechol groups for grafting. Furthermore, the trends for both MPC-100 and POEGMA-100 essentially overlap, and may reflect the fact that both data series employed the same silane surface anchor. (It might also reflect the fact that both series used the same methyl acrylate polymer backbone.)

4. Comparison of fibroblast mammalian cell attachment adsorption on PSAR-20 and on POEGMA surface grafted polymer brushes

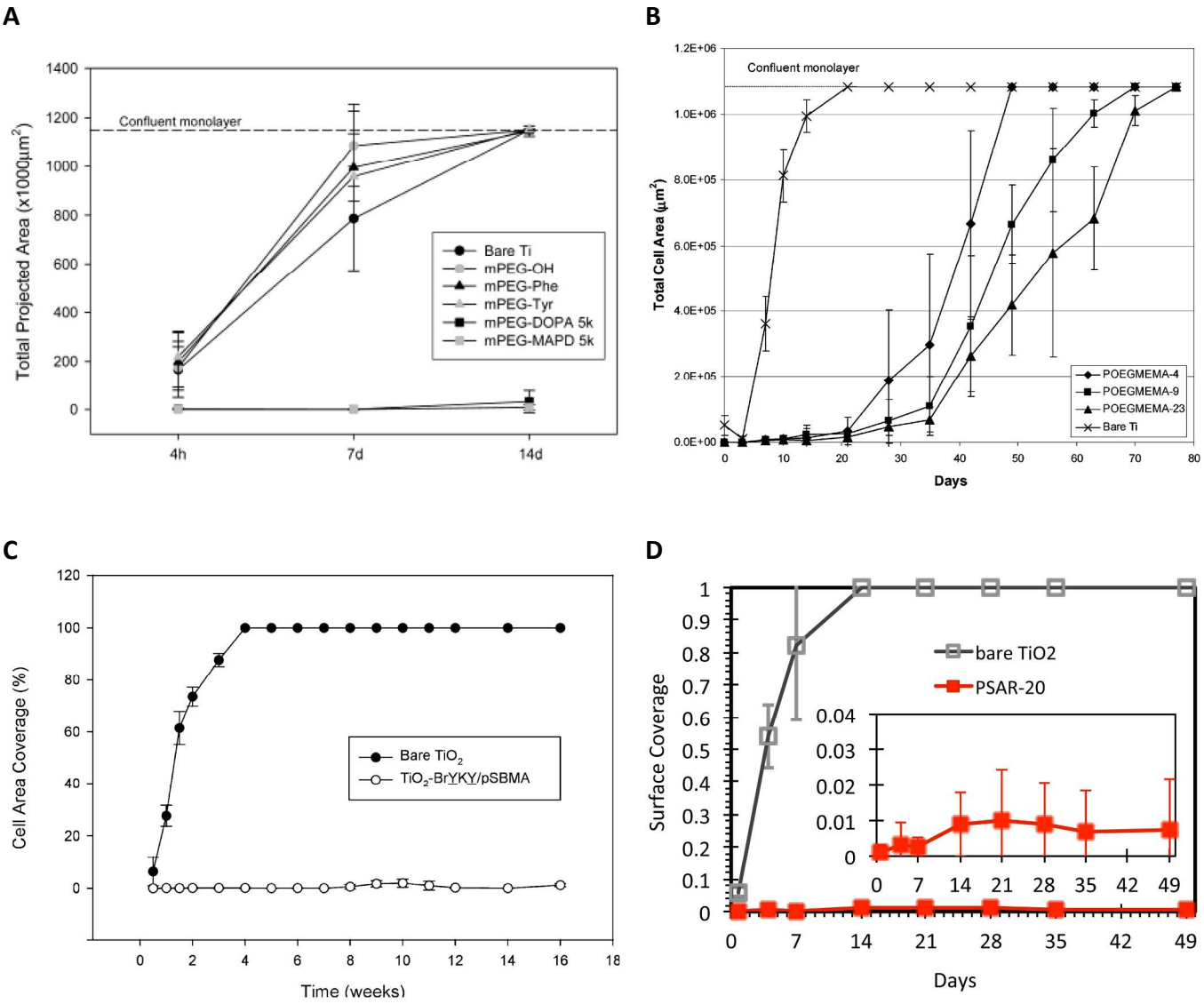

Figure S4. Long-term fibroblast attachment experiment on surfaces grafted with (A) methoxy-terminated poly(ethylene glycol) (mPEG, $M_w \approx 5$ kDa, reproduced from Dalsin et al.[7], (B) acrylate polymer with oligo(ethylene glycol) methyl ether methacrylate monomers (POEGMEMA, layer thickness ≈ 100 nm) reproduced from Fan et al.[8]), (C) acrylate polymer with zwitterionic sulfobetaine methacrylate monomters (pSBMA, layer thickness ≈ 15 nm) reproduced from Kuang et al.,[9] and (D) PSAR-20 (reproduced from Figure 5A in the main text). All experiments were conducted with 3T3 mouse fibroblasts and cells were reseeded at least twice weekly on the substrates (see Experimental in the main text). In (A), the suffix to POEGMEMA denotes the average number of ethylene glycol units in the sidechain. In (B), the suffixes to mPEG denote the terminal chemistry of the methoxy-capped PEG chains: -OH = hydroxyl group; -Phe = the amino acid phenylalanine; -Tyr = the amino acid alanine; -DOPA = the amino acid 3,4-dohydroxy phenylalanine; -MAPD = a mussel adhesive protein mimetic peptide sequence that includes a terminal DOPA residue. Only the MAPD and DOPA termini were designed to graft the mPEG-5k to the TiO_2 surface. The error bars indicate ±1 SD.

The ability of mouse fibroblasts to attach and proliferate on PSAR-20 is compared with that on PEG, POEGMEMA, and zwitterionic pSBMA polymer brushes in Figure S4. Fibroblast attachment and and subsequent proliferation and growth on the bare TiO_2 control surfaces steadily increased through the first 2 weeks of experiments, reaching at least 70% coverage by day 14 in all experiments (the bare Ti in Figures S4A and B were each also covered with a layer of TiO_2 native oxide). In contrast, all polymer

brushes with proper surface grafting chemical groups (mPEG-DOPA, mPEG-MAPD, all POEMEMA, pSBMA and PSAR-20) were able to essentially inhibit fibroblast attachment and growth completely in this period. By 14 d, there was a very small increase to 1~2% surface coverage on all the grafted polymer surfaces except for mPEG-MAPD and pSBMA, on which fibroblast attachment was still negligible. Notwithstanding, within experimental uncertainty, PEG-5k, POEGMEMA, pSBMA and PSAR-20 were all able to inhibit fibroblast attachment for at least 2 wk.

Data is not available after 14d for PEG. PSAR-20 is shown to inhibit fibroblast attachment at a very low level of ~1% surface coverage up to the last time point for which data is available (49 d; 7 wk), while pSBMA was shown to inhibit fibroblast attachment up to 16 wk. In comparison, fibroblast attachment grew to significant levels on POEGMEMA by day 28. Fibroblast growth on POEGMEMA-4 reach full coverage by 7 wk, while POEGMEMA-23 with longer sidechains was able delay growth to full coverage until the 11^{th} wk. Superficially, therefore, PSAR-20 and pSBMA appear to offer better resistance against fibroblast attachment than POEGMEMA over periods longer than 2 wk. No conclusion is drawn for PEG for this time-scale due to the lack of data. However, the above analysis must be treated with caution, as the data could simply reflect differences in the stability of the different anchoring mechanisms used for the different polymer brushes (presumably less stable in the case of the POEGMEMA brushes, with more significant decreases in the grafted brush density over time).

5. AFM measurements on TiO_2 (in air) and on PSAR-20 brush (in aqueous solution)

Atomic force microscopy (AFM) measurements were performed on a MFP3D instrument (Asylum, Santa Barbara, CA). Silicon cantilevers (80 kHz, nominally 0.6 N/m in air; Mikromasch, Santa Barbara, CA) were used for both tapping and contact mode measurements in liquid. Silicon cantilevers (60 kHz, nominally 2 N/m; also from Mikromasch) were used for tapping-mode measurements in air. For liquid measurements, the samples were immersed in 100 mM KCl solutions at pH 7, with pH adjusted by addition of HCl and KOH. Cantilever bending stiffness calibration was performed using the frequency domain thermal noise sweep included with the software for controlling the MFP3D instrument. The cantilever-tip used for liquid AFM scratching experiments was measured to have a resonance frequency in 100 mM KCl = 46.6 kHz, bending-sensor response = 113 nm/V and stiffness = 3.0 nN/nm.

The liquid AFM measurements reveal a smooth PSAR-20 surface when grafted at 0.82 nm^{-2} and did not reveal any obvious defects in the brush layer (Figure S5). The height range of the PSAR-20 brush was < 1 nm, while the height range of the underlying TiO_2 substrate grain structure was ~2 nm (Figure S6). This shows that the dynamic PSAR-20 brush completely covered the TiO_2 surface and was able to obscure the underlying topography as seen by the AFM probe (~5 nm radius). However, the spatial resolution of liquid AFM on these non-atomically flat substrates may be too low to resolve features less than ~5 nm in size. It also would not be able to resolve any molecular aggregation, if present, on PSAR surfaces grafted at lower chain densities, and measurements on those samples were not performed.

AFM contact mode "scratching" experiments (Figure S7) also revealed a minimum wet thickness of ~6 nm for the 0.82 nm-2 PSAR-20 brush (dry thickness = 2.2 nm). The contour length of the polysarcosine 20-mer is 6.8 nm, and that of the DOPA-Lys pentapeptide anchor is 1.7 nm (using the value of 0.34 nm per residue for amino acids). A defect in the PSAR-20 brush was first made by scanning a 0.5 x 0.5 μm^2 area in contact mode at high force, which was then imaged when scanned over a larger area in tapping mode, using a much reduced, intermittent force, to reveal both the defect and the intact surrounding brush layer.

After scratching at a relatively low force of 500 nN, a defect with a depth of ~2.5 nm was measured (Figure S7A and C). At a higher applied force of 1.7 μN, a depth of ~6 nm was measured (Figure S7B and D). Note that the larger amount of material removed at a higher force (see the larger amount of debris in Figure S7B compared with S7A) is consistent with the removal of a soft polymer layer; the Si tip is not stiff enough to remove the underlying TiO_2 substrate. Measurements at an even higher force were not attempted because scratching at 1.7 μN already induced a large amount of debris that made high resolution imaging difficult (see the longer traces/"shadows" of features in Figure S7B compared with S7A that is partially obscuring the bottom of the defects).

The absolute wet thickness of the PSAR-20 brush is a difficult quantity to measure. In AFM, the height position of the (dynamic) polymer brush depends on the force applied by the AFM tip during imaging, and AFM scratching cannot guarantee that all the polymer material has been displaced with the AFM tip. Other measurement techniques must also contend with defining the brush "height", as the fraction of space occupied by the polymer brush is a distribution that has a maximum close to the grafting surface and that decays towards the maximum height allowed by the polymer contour length.

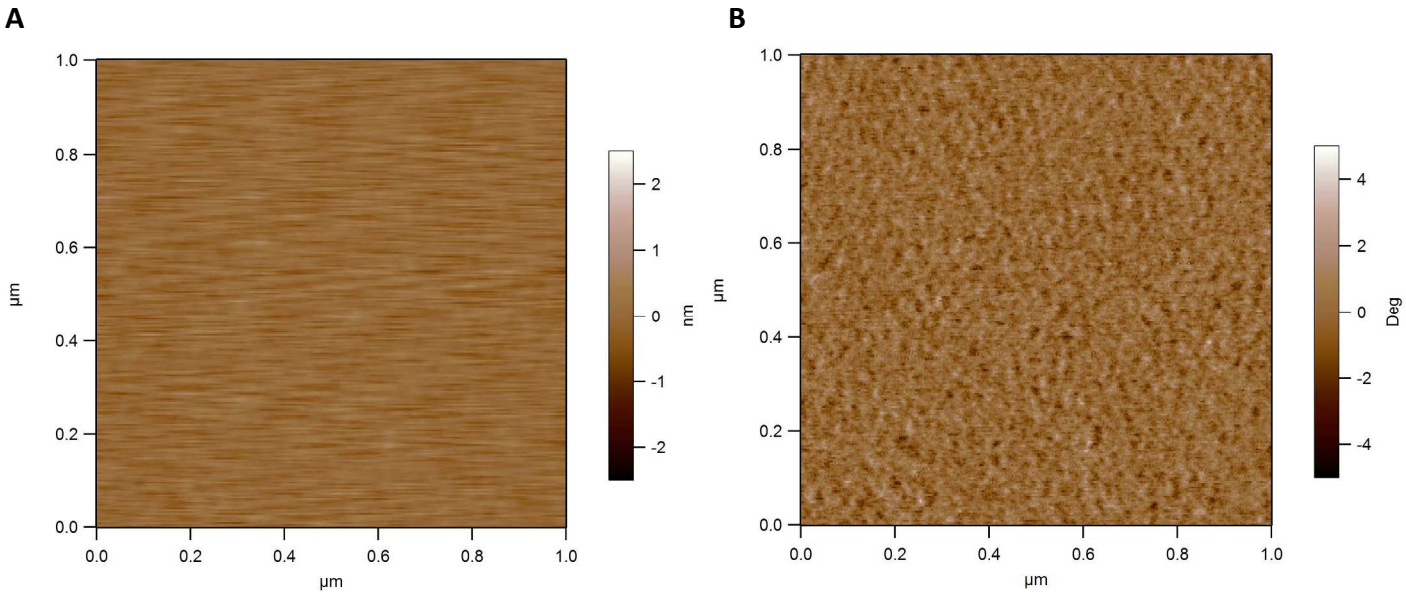

Figure S6. Typical tapping mode liquid AFM images obtained in 100 mM KCl (pH 7) of the PSAR-20 brush layers (dry thickness = 2.2 nm; 0.82 nm^{-2}) immobilized on the TiO_2 substrate shown in Figure S5. (A) shows the topography image of a scan area of 1x1 μm^2, while (B) shows the corresponding phase image of the same area. As is common in tapping mode AFM, the phase image reveals the stiffness response of the surface and thereby reveals lateral details of surface that may be obscured by differences in height topography. Neither the topography nor the phase image shows any obvious defects ("holes") in the PSAR-20 brush layer. The height range of the brush surface is < 1 nm, and is much reduced compared to the underlying grain structure (see Figure S5A).

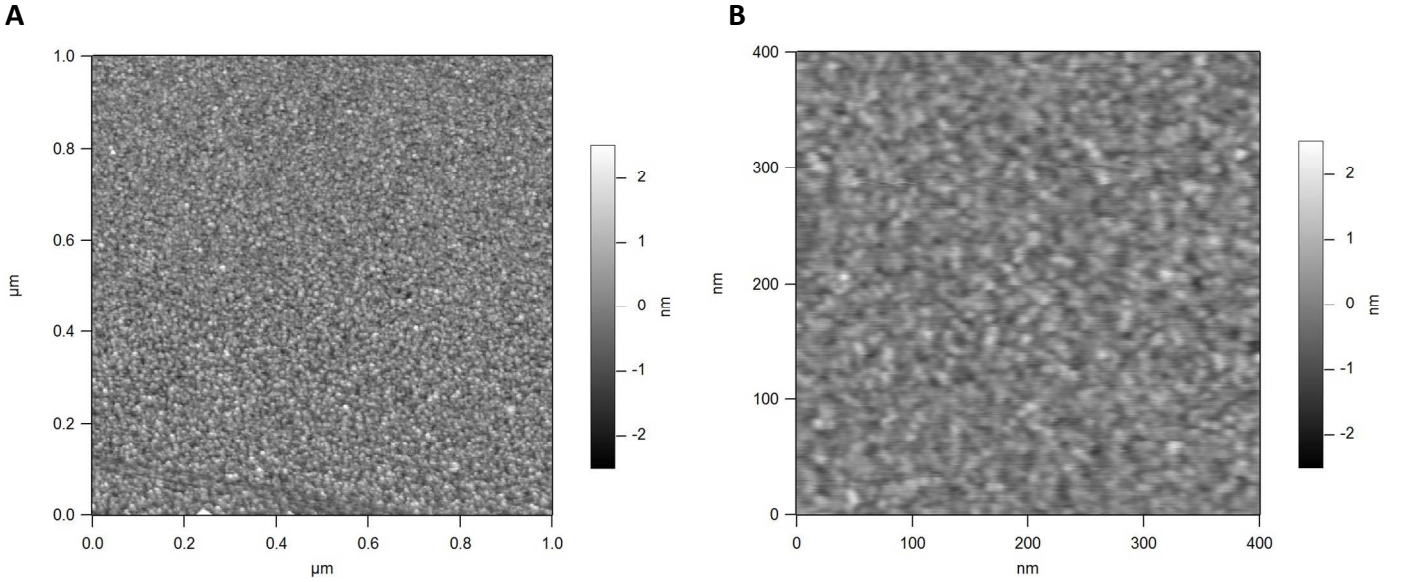

Figure S5. Typical tapping mode AFM images obtained in air of the TiO_2 layers deposited on silicon substrates. (A) shows a scan area of 1x1 μm^2, while (B) shows another area at a higher magnification (0.5x0.5 μm^2). Grains of ~5 nm in diameter can be observed on these polycrystalline films. The height range of the grain structure spans ~2 nm over an area of 1 μm^2.

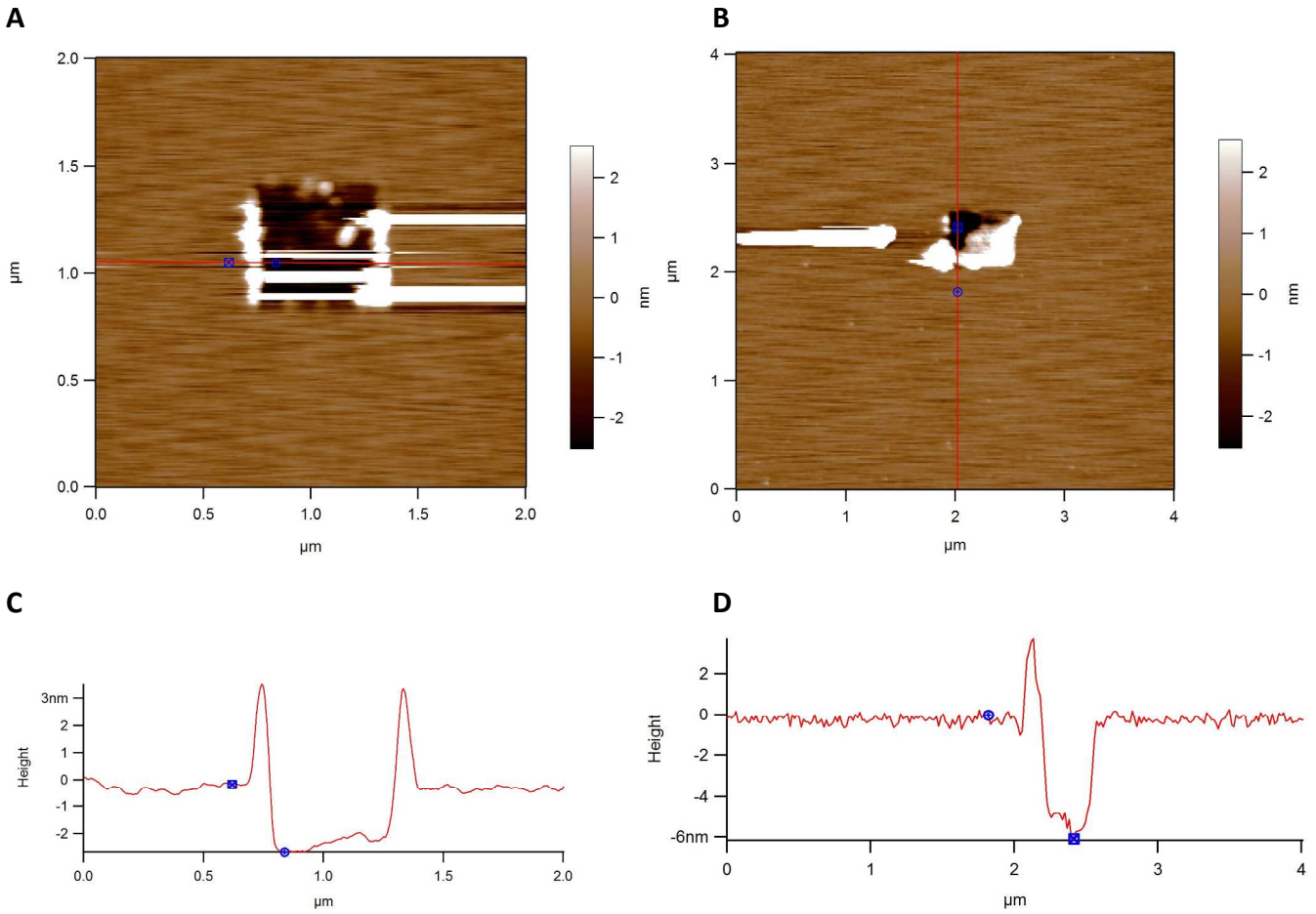

Figure S7. Liquid AFM scratching measurement of the wet PSAR-20 brush thickness. A defect in the PSAR-20 brush was first made by scanning a 0.5 x 0.5 μm^2 area in contact mode at high force, which was then imaged when scanned over a larger area in tapping mode, using a much reduced, intermittent force, to reveal both the defect and the intact surrounding brush layer. (A) shows a 0.5 x 0.5 μm^2 defect made at 500 nN and imaged over a 2 x 2 μm^2 area, while (B) shows a second 0.5 x 0.5 μm^2 defect made on another area of the sample, at a 333% higher force of 1.7 µN and imaged over a 4 x 4 μm^2 area. The red linear traces in (A) and (B) correspond to where cross-sections of the defects were measured and shown, respectively, in panels (C) and (D). It is seen that the depth of the defect made at 500 nN was ~2.5 nm, and the depth of the defect made at 1.7 µN was ~6 nm.

6. Adsorption measurements on PSAR-20 samples immersed in 10% bovine serum

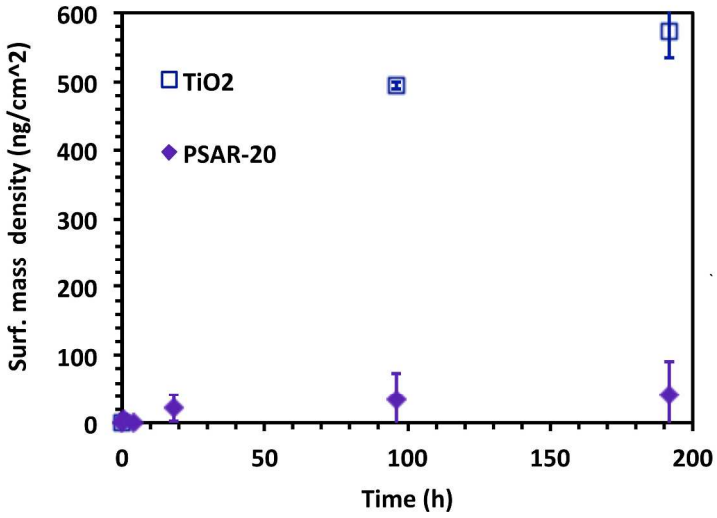

Figure S8. Adsorption of cell culture media material on PSAR-20 (initial grafting density of 0.87 nm^{-2}) over 8 d. The cell culture media used is the same as that used for the long-term fibroblast culture on PSAR-20 (Figure 6 in the main text), and is composed of Dulbecco Modified Eagle's Media (DMEM) added with antibiotics and bovine serum to a total concentration of 10% (see Experimental in the main text for details). The measurement approach used for the fibrinogen adsorption experiment described in the main text is also employed here. Briefly, PSAR coated TiO_2 samples were immersed in the media using 24-well plates, and placed in the cell culture incubator at 37°C, for the duration of the experiment. They were then rinsed with UP H2O, and dried under a stream of N_2 for measurement by ellipsometry in air. The amount of adsorbed proteins was obtained from ellipsometer measurements of the adlayer thickness relative to the peptoid brush thickness of the control immersed in unloaded buffer. Samples immersed in 10 mM HEPES buffer added with 150 mM NaCl at an original pH = 7.4 under ambient conditions were used as controls. Individual sample sets were used to obtain the data for each time point (20 min, 2h, 18h, 4 d and 8 d). N = 3. To fall in line with the cell culture protocol, the immersion media were exchanged a fresh batch every 3 d (for the 4 and 8 d samples). The error bars indicate ±1 SD.

References

1. Saxer, S.; Portmann, C.; Tosatti, S.; Gademann, K.; Zuercher, S.; Textor, M., Surface Assembly of Catechol-Functionalized Poly(L-lysine)-graft-poly(ethylene glycol) Copolymer on Titanium Exploiting Combined Electrostatically Driven Self-Organization and Blomimetic Strong Adhesion. *Macromolecules* **2010,** *43* (2), 1050-1060.
2. Pei, J.; Hall, H.; Spencer, N. D., The role of plasma proteins in cell adhesion to PEG surface-density-gradient-modified titanium oxide. *Biomaterials* **2011,** *32* (34), 8968-8978.
3. Feng, W.; Zhu, S. P.; Ishihara, K.; Brash, J. L., Protein resistant surfaces: Comparison of acrylate graft polymers bearing oligo-ethylene oxide and phosphorylcholine side chains. *Biointerphases* **2006,** *1* (1), 50-60.
4. Lau, K. H. A.; Ren, C.; Park, S. H.; Szleifer, I.; Messersmith, P. B., An Experimental–Theoretical Analysis of Protein Adsorption on Peptidomimetic Polymer Brushes. *Langmuir* **2012,** *28* (4), 2288-2298.
5. Szleifer, I., Protein Adsorption on Surfaces with Grafted Polymers: A Theoretical Approach. *Biophys. J.* **1997,** *72* (2_Pt_1), 595-612.
6. Satulovsky, J.; Carignano, M. A.; Szleifer, I., Kinetic and thermodynamic control of protein adsorption. *Proc. Natl. Acad. Sci. USA* **2000,** *97* (16), 9037-9041.
7. Dalsin, J. L.; Hu, B.-H.; Lee, B. P.; Messersmith, P. B., Mussel Adhesive Protein Mimetic Polymers for the Preparation of Nonfouling Surfaces. *J. Am. Chem. Soc.* **2003,** *125* (14), 4253-4258.
8. Fan, X.; Lin, L.; Messersmith, P. B., Cell Fouling Resistance of Polymer Brushes Grafted from Ti Substrates by Surface-Initiated Polymerization: Effect of Ethylene Glycol Side Chain Length. *Biomacromolecules* **2006,** *7* (8), 2443-2448.
9. Kuang, J.; Messersmith, P. B., Universal Surface-Initiated Polymerization of Antifouling Zwitterionic Brushes Using a Mussel-Mimetic Peptide Initiator. *Langmuir* **2012,** *28* (18), 7258-7266.